

# Mathematical modeling of tomographic scanning of cylindrically shaped test objects

**B I Kapranov, G V Vavilova, A V Volchkova and I S Kuznetsova**

National Research Tomsk Polytechnic University, Tomsk, Russia

E-mail: wgw@tpu.ru

**Abstract.** The paper formulates mathematical relationships that describe the length of the radiation absorption band in the test object for the first generation tomographic scan scheme. A cylindrically shaped test object containing an arbitrary number of standard circular irregularities is used to perform mathematical modeling. The obtained mathematical relationships are corrected with respect to chemical composition and density of the test object material. The equations are derived to calculate the resulting attenuation radiation from cobalt-60 isotope when passing through the test object. An algorithm to calculate the radiation flux intensity is provided. The presented graphs describe the dependence of the change in the  $\gamma$ -quantum flux intensity on the change in the radiation source position and the scanning angle of the test object.

## 1. Introduction

The analysis of the internal structure of the test object is required to solve various problems of non-destructive testing [1–6]. X-ray tomography uses X-rays. The initial data for the analysis of the object internal structure are projections (X-ray patterns). An X-ray pattern is a two-dimensional shadow image. The structural elements in the image overlap, which does not allow examination and comparison of individual local fragments [7–8] in different parameters. However, if an X-ray pattern is produced from different directions, more data on the object internal structure can be obtained [9, 10].

This problem can be solved by means of X-ray computed tomography [11, 12]. The X-ray computed tomography measures spatial distribution of a specific physical quantity from different directions and computes the images free of interference caused by overlapped structures [7, 9, 13].

The main components of the X-ray tomograph are a tube, a detector and a rotary mechanism [11, 13–15]. To obtain a tomographic image, the test object is placed between the tube and the detector. During scanning, the test object is rotated by  $360^\circ$  [11, 16]. X-rays interact with the test object material and form its shadow image on the detector. Thus, a set of shadow images of the scanned object is obtained, and the array of the images is used for mathematical reconstruction of the object cross section [17].

This paper describes a program for modeling tomographic scanning in first-generation geometry, i.e. the source is regarded as a point  $\gamma$ -ray source.

In survey radiography, a relative X-ray intensity distribution is recorded. The radiation intensity of the detector decreases exponentially as the scanned sample thickness increases [18].



**2. Geometry of test object scanning**

To write algorithms and programs for collecting projection data and mathematical reconstruction, tomography uses test objects that have a set of standard inhomogeneities with designed geometric dimensions located within the reconstruction zone [19–21].

Figure 1a shows the section of a cylindrically shaped test object with the radius  $r_0$  base.

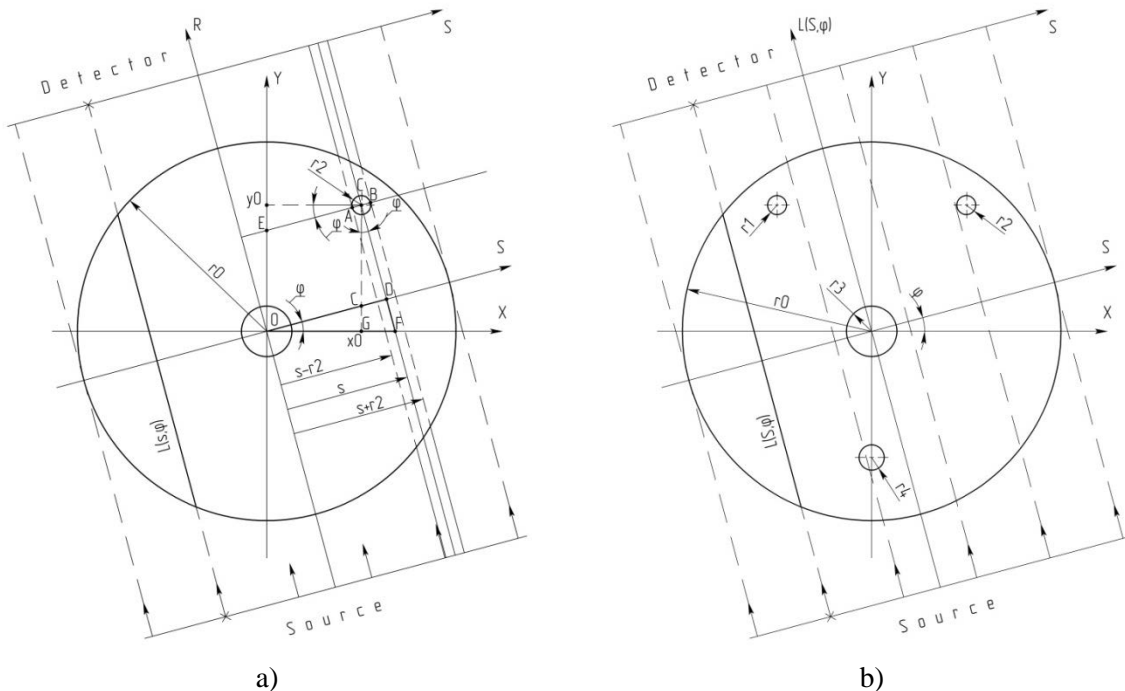


**Figure 1.** Geometry of the test object cross section, where  $X$  and  $Y$  are coordinate axes in the Cartesian coordinate system;  $x$  and  $y$  are distances to an arbitrary point in the Cartesian coordinate system;  $S$  and  $R$  are coordinate axes in the scanning system;  $s$  and  $r$  are distances to an arbitrary point in the scanning system;  $\varphi$  is the angle of the scanning system rotation with respect to the Cartesian coordinate system.

The test object center coincides with the reconstruction zone center ( $t.0$ ). The hole center with radius  $r_2$  lies in the  $XY$  plane at point  $(x_0, y_0)$ .

For computational convenience, turn from the Cartesian coordinate system to the polar coordinate system. In this case, the coordinate axes of the Cartesian coordinate system ( $X$  and  $Y$ ) are replaced by the coordinate axes in the scanning system ( $S$  and  $R$ ) through the system rotation by angle  $\varphi$ . Then the hole center with radius  $r_2$  in the scanning system ( $SR$  plane) is located at point  $(s, r)$ , the value of which depends on rotation angle  $\varphi$ .

The source radiation absorption intensity largely depends on the test object thickness. In the presented geometry (see Figure 1a), the test object thickness changes as it moves along the  $S$  axis, i.e. the test object thickness is equal to the circle chord length  $L(s)$ .

For a circle with radius  $r_0$  (in case of holes inside it), the chord length is calculated by equation [18]:

$$L(s) = 2r_0 \cdot \sqrt{1 - \left(\frac{s}{r_0}\right)^2} \tag{1}$$

where  $r_0$  is the test object radius;  $s$  is the distance to an arbitrary point in the scanning system through which the chord passes.

The holes in the test object decrease the test object thickness, i.e. the chord length reduces. To find the resulting chord length in case of a hole inside the object, consider the hole with radius  $r_2$  in Figure 1a.

To find the  $OD$  distance (the position of the center in the hole with radius  $r_2$  on the  $S$  axis), one must know the length of the segment  $OF$  (projection of the position of the center in the hole with radius  $r_2$  on the  $X$  axis). To find the length, consider the  $\triangle DOF$  triangle. Since  $\frac{OD}{OF} = \cos \varphi$ , then

$$OD = OF \cdot \cos \varphi . \quad (2)$$

The  $OF$  segment consists of two segments  $OG$  and  $GF$ . According to Figure 1a, the segment  $OG = x_0$ , hence

$$OF = x_0 + GF . \quad (3)$$

According to the theorem on the equality of angles with mutually perpendicular sides,  $\angle GCF$  is equal to angle  $\varphi$  (see Figure 1a). In this case  $\operatorname{tg} \varphi = \frac{GF}{CG} = \frac{GF}{y_0}$ . Hence

$$GF = y_0 \cdot \operatorname{tg} \varphi . \quad (4)$$

Substitute expression (4) into (3) to have the expression for the segment  $OF$  in the form [9]:

$$OF = x_0 + y_0 \cdot \operatorname{tg} \varphi . \quad (5)$$

Substitute the obtained data (5) into (2), and it turns out that

$$OD = OF \cdot \cos \varphi = (x_0 + y_0 \cdot \operatorname{tg} \varphi) \cdot \cos \varphi = x_0 \cdot \cos \varphi + y_0 \cdot \sin \varphi .$$

Consequently, the coordinates of the hole center in the scanning system depend on angle  $\varphi$  and can be calculated by the equation:

$$s(\varphi) = x_0 \cdot \cos \varphi + y_0 \cdot \sin \varphi . \quad (6)$$

The hole chord length  $l(\varphi, s)$  depends on angle  $\varphi$  and on the distance to the hole center  $s$ . For the given angle  $\varphi$ , the chord length  $l$  of hole  $r_2$  (Figure 1a) takes the maximum value equal to  $2 \cdot r_2$  if  $s = x_0 \cdot \cos \varphi + y_0 \cdot \sin \varphi$  (in the hole center), and it is of minimum value equal to zero if  $s = [x_0 \cdot \cos \varphi + y_0 \cdot \sin \varphi] - r_2$  and  $s = [x_0 \cdot \cos \varphi + y_0 \cdot \sin \varphi] + r_2$  (at the hole edges) [9, 13].

Similarly to (1), the hole chord length is described by the expression

$$l(s, \varphi) = 2 \cdot r_2 \cdot \sqrt{1 - \left[ \frac{s - (x_0 \cdot \cos \varphi + y_0 \cdot \sin \varphi)}{r_2} \right]^2} , \quad (7)$$

where  $s$  is distances to an arbitrary point in the scanning system;  $r_2$  is the radius of the hole in question.

The presence of a hole decreases the chord length, which can be calculated by the equation:

$$Ll(s, \varphi) = L(s, \varphi) - l(s, \varphi) . \quad (8)$$

### 3. Calculation of radiation intensity attenuation

In survey radiography, relative X-ray intensity distribution is recorded. To calculate the attenuation coefficient, it is necessary to measure both the primary radiation intensity (from the source) and the detector radiation intensity, which decreases exponentially as the thickness of the scanned object increases [18, 22].

The resulting radiation attenuation along the ray path through the object is determined by the dependence

$$P(s, \varphi) = P_0 e^{-\int_0^L \mu[l(s, \varphi)] dl} , \quad (9)$$

where  $P_0$  is the radiation source intensity;  $P(s, \varphi)$  is the radiation intensity of the detector;  $\mu[l(s, \varphi)]$  is linear radiation attenuation coefficient at point  $l$  along ray  $L(s, \varphi)$ .

Linear attenuation coefficient  $\mu$  depends on medium density  $\rho$  and mass attenuation coefficient  $\mu_p$

$$\mu = \mu_p \cdot \rho \quad (10)$$

Mass attenuation coefficient  $\mu_p$  is determined by chemical composition of the substance, photo absorption cross sections  $\tau$ , Compton scattering  $\sigma$ , and pairing  $\alpha$  for each of the constituent elements, which values depend on radiation energy  $E$ . The total mass attenuation coefficient is calculated by the equation  $\mu_p = \sum_i \omega_i \cdot \mu_p^i$ .

where  $\omega_i$ , % is percentage content of the  $i$ -th element in the substance of the test object.

For the test object without any holes inside, but taking into account the attenuation coefficient, equation (1) can be written in the form

$$L(s) = 2\mu_0 \cdot r_0 \sqrt{1 - \left(\frac{s}{r_0}\right)^2}, \quad (11)$$

where  $\mu_0$  is the linear coefficient of radiation attenuation of the test object material.

The  $\gamma$ -quantum flux intensity can be also affected by holes inside the test object. Taking into account the linear radiation attenuation coefficient of the hole materials, equation (7) takes the form (similar to (1) and (11))

$$l(s, \varphi, \mu_i) = 2 \cdot r_i \cdot \mu_i \sqrt{1 - \left[ \frac{s - (x_i \cdot \cos \varphi + y_i \cdot \sin \varphi)}{r_i^2} \right]^2}, \quad (12)$$

where  $s$ , is distances to an arbitrary point in the scanning system;  $r_i$  is the radius of the hole in question.

The presence of a hole decreases the length of the ray along which radiation propagates. In the presence of  $n$  holes, taking into account the attenuation coefficients of each hole, the total decrease in the ray length can be calculated by the equation similar to (8):

$$Ll(s, \varphi, R_i, \mu_i) = L0(s, \varphi, \mu_0) - \sum_{i=1}^n l(s, \varphi, \mu_i), \quad (13)$$

where  $n$  is the number of holes;  $R_{0i}$  is the position of the  $i$ -th hole center;  $\mu_i$  is attenuation coefficient of each hole;  $\varphi$  is projection angle (from 0 to  $2\pi$ );  $r_i$  is the radius of the  $i$ -th hole.

During transition from the Cartesian coordinate system to the polar one, coordinates of any point  $(x_i, y_i)$  can be converted into value  $R$ . According to the Pythagorean theorem, it can be calculated by the equation  $R_i = \sqrt{x_i^2 + y_i^2}$ .

Then expression (7) can be written in the form  $l(s, \varphi, \mu_i) = 2 \cdot r_i \cdot \mu_i \sqrt{1 - \left[ \frac{s - R_i \cdot \cos \varphi}{r_i^2} \right]^2}$ , where  $s$ , is

distances to an arbitrary point in the scanning system;  $r_i$  is the radius of the hole in question;  $R_i$  is the distance to the hole center.

#### 4. Geometry of the test object scanning

Cylindrical test objects with a set of standard inhomogeneities with known geometric dimensions located within the reconstruction zone are used to develop algorithms and programs for collecting projection data in the reconstruction tomography [13, 23].

The studied test object is a cylinder with a base radius  $r0 = 30$  cm with 4 round holes. The radii and coordinates of the centers are equal to:  $r1 = 1.5$  cm, point A1 (-15; 20);  $r2 = 1.5$  cm, point A2 (15; 20);  $r3 = 4$  cm, point A3 (0; 0);  $r4 = 2$  cm, and point A4 (0; 20) (Figure 1b).

The positions of the hole centers in the new coordinate system are found by the Pythagorean theorem ( $R_1 = 25$  cm,  $R_2 = 25$  cm,  $R_3 = 0$  cm, and  $R_4 = 20$  cm). The displacement angle of each hole relative to the origin is equal to:  $\theta_1 = \pi - \arctg\left(\frac{20}{15}\right)$ ,  $\theta_2 = \arctg\left(\frac{20}{15}\right)$ ,  $\theta_3 = 0$ , and  $\theta_4 = \frac{3\pi}{2}$ .

The chemical composition of the test-object material can be described by the formula  $Ba(NO_3)_2 + C_6H_{10}O_5$ . The composition density is  $\rho = 1.8$  g/cm<sup>3</sup>. Since the paper considers only one arbitrary section of the object, the object height is not of interest to us.

Isotope cobalt-60 ( $Co^{60}$ ) is used as a radiation source, which  $\gamma$ -radiation comprises two 1.173 MeV and 1.332 MeV lines located side by side. Therefore,  $\gamma$ -radiation from  $Co^{60}$  is considered to be monochromatic at energy  $E_0=1.25$  MeV [11].

Table 1 summarizes the values for mass coefficients of radiation attenuation and the percentage content for each chemical element found in the test object material at energy of 1.25 MeV [16].

Using the data from Table 1 and equation (11), the mass attenuation coefficient for the test object material can be calculated by

$$\mu_p = \omega(H) \cdot \mu_p(H) + \omega(O) \cdot \mu_p(O) + \omega(C) \cdot \mu_p(C) + \omega(N) \cdot \mu_p(N) + \omega(Ba) \cdot \mu_p(Ba) = 0.056 \text{ cm}^2/\text{g}.$$

The linear attenuation coefficient of the test object material is calculated by equation (10)

$$\mu = \mu_p \cdot \rho = 0.056 \cdot 1.8 = 0.1013 \text{ sm}^{-1}.$$

The initial attenuation coefficients for each hole are determined in a similar manner and are equal to:  $\mu_0=0.3$ ,  $\mu_1=0.1$ ,  $\mu_2=0.1$ ,  $\mu_3=0$  and  $\mu_4=0$ , respectively.

The equation similar to (9) can be used to calculate the detector radiation intensity in Mathcad

$$P = P_0 \cdot e^k, \tag{11}$$

where  $k = -Ll(x_i, \varphi, r0, r_i)$ , (13);  $x_i = -r0 + 2\frac{r0i}{n}$  are coordinates of an arbitrary point from  $-r0$  to  $r0$  cm [19, 24].

**Table 1.** Content of chemical elements and their mass attenuation coefficients for  $Ba(NO_3)_2 + C_6H_{10}O_5$

Element	Percentage, $\omega, \%$	Mass attenuation coefficient, $\mu_p, \text{cm}^2/\text{g}$
H	3	0.114
O	41	0.054
C	15	0.062
N	7	0.055
Ba	34	0.052

The scanning angle range  $\varphi$  from 0 to  $2\pi$  is used to perform calculations. Figures 2–5 illustrate changes in the detector radiation intensity when the point source changes its position within a range from  $-30$  to  $30$  cm (the test object size in the section plane) for scanning angles 0,  $\pi/4$ ,  $\pi/2$  and  $\pi$ , respectively.

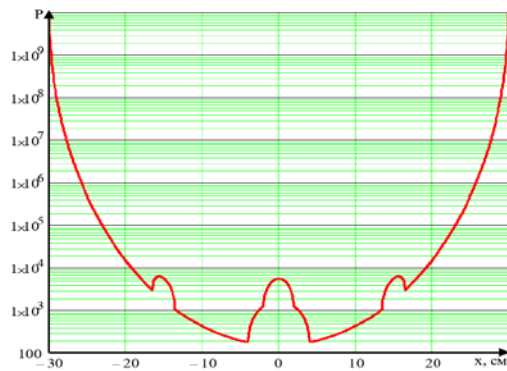


**Figure 2.** Graph of the change in the  $\gamma$ -quantum flux intensity when the scanning line changes its position from  $-30$  to  $30$  cm for scanning angle  $\varphi = 0$

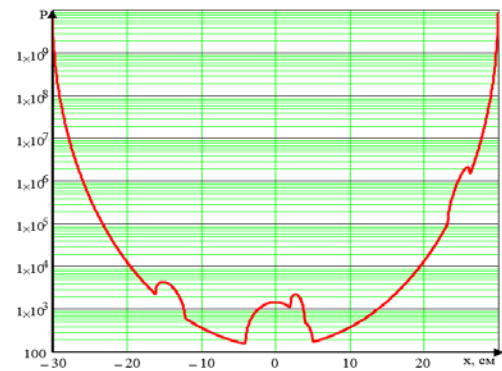


**Figure 3.** Graph of the change in the  $\gamma$ -quantum flux intensity when the scanning line changes its position from  $-30$  to  $30$  cm for scanning angle  $\varphi = \pi / 4$

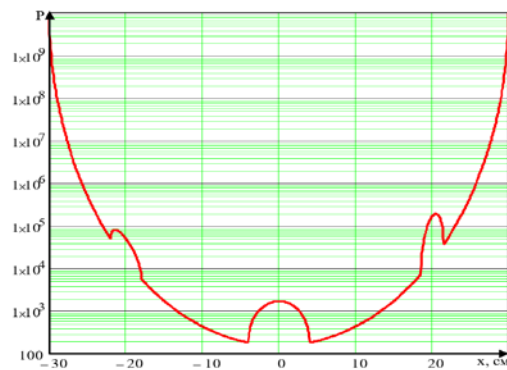


**Figure 4.** Graph of the change in the  $\gamma$ -quantum flux intensity when the scanning line changes its position from  $-30$  to  $30$  cm for scanning angle  $\varphi = \pi / 2$

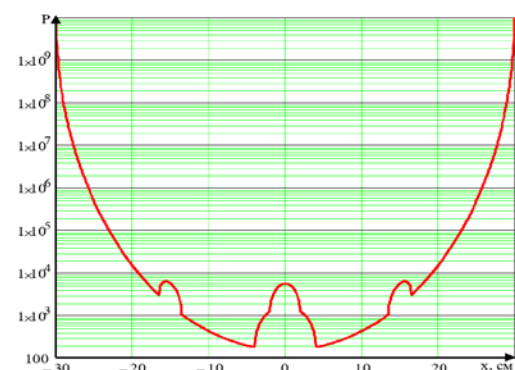


**Figure 5.** Graph of the change in the  $\gamma$ -quantum flux intensity when the scanning line changes its position from  $-30$  to  $30$  cm for scanning angle  $\varphi = \pi$

The graphs show that the presented calculations can be used to easily detect the position of internal holes and to determine their size and structure (by analyzing the attenuation coefficient). The graphs for different scanning angles make it possible to reveal the internal structure of the object scanned.

## 5. Conclusion

1. The mathematical relationships describing the length of the absorption line in cylindrical test objects are defined. Test objects containing an arbitrary number of standard irregularities of circular shape are used for scanning.
2. The obtained mathematical relationships describing the length of the absorption line of  $\gamma$ -quantum coming from  $\text{Co}^{60}$  isotope are corrected, taking into account the attenuation coefficient for the material with known chemical composition and density.
3. An algorithm for calculating the length of radiation ray passing through the test object with an arbitrary number of standard irregularities of circular shape, which is made of the material of the known chemical composition and density, is provided.
4. Test calculations are performed for several projection angles to show the possibility of modeling the process of collecting projection data for arbitrary sizes and locations of inhomogeneity's in the test object.

## References

- [1] Hussein E M A 2011 *Computed Radiation Imaging. Physics and Mathematics of Forward and Inverse Problems* (Elsevier: Netherlands)
- [2] Gradoboev A V and Orlova K N 2014 *Adv Mater Res* **880** 237–241 doi: 10.4028/www.scientific.net/AMR.880.237
- [3] Payuk L A et al 2016 *J Phys: Conf Series* **671(1)** 012044 doi: 10.1088/1742-6596/671/1/012044
- [4] Karlova G F and Gradoboev A V 2013 *Proc of SIBCON'2013* 6693581 doi: 10.1109/SIBCON.2013.6693581
- [5] Surzhikov A P et al 2016 *IOP Conf Ser: Mater Sci Eng* **110(1)** 012002 doi: 10.1088/1757-899X/110/1/012002
- [6] Plotnikova I V et al 2018 *IOP Conf Ser: Mater Sci Eng* **289(1)** 012029 doi:10.1088/1757-899X/289/1/012029
- [7] Hemmy D et al 1983 *Neurosurgery* **13(5)** 534–541
- [8] Vavilova G V and Ryumkin A V 2018 *IOP Conf Ser: Mater Sci Eng* **289(1)** 012017 doi: 10.1088/1757-899X/289/1/012017
- [9] Natterer F 1990 *The mathematics of computerized tomography* (Stuttgart: John Wiley & Sons)
- [10] Grangeat P 1990 *Proc of Conf Mathematical Methods in Tomography* (Oberwolfach, Germany) 66–97
- [11] Carmignato S et al (eds) 2018 *Industrial X-Ray Computed Tomography* (Springer International Publishing AG: Switzerland) 185–228 doi: 10.1007/978-3-319-59573-3\_5
- [12] Brenner D J and Hall E J 2007 *N Engl J Med* **357** 2277–2284
- [13] Nizhegorodov A I et al 2017 *IOP Conf Ser: Mater Sci Eng* **289(1)** 012014 doi:10.1088/1757-899X/289/1/012014
- [14] Coles M E et al 1994 *Proc of Annual SCA Meeting* 12–14
- [15] Plotnikova I et al 2018 *MATEC Web of Conferences* **155** 01052 doi: 10.1051/mateconf/201815501052
- [16] Storm E and Israel H 1967 *Photon cross sections from 0,001 to 100 Mev for elements 1 through 100* (Los Alamos: Los Alamos Scientific Laboratories)
- [17] Vishnyakov G N et al 2004 *Microscopy and Analysis* **18(1)** 15–17
- [18] Hansell D M 2001 *Eur Radiol* **9** 1666–1680
- [19] Bakulin V N et al 2015 *J Eng Phys Thermophys* **88(2)** 556–560 doi: 10.1007/s10891-015-1221-7
- [20] Sarsikeev Y et al 2014 *Advanced Materials Research* **953–954** 529–532 doi: 10.4028/www.scientific.net/AMR.953-954.529
- [21] Uglov V V et al 2013 *Russ J Non Ferr Met+* **54(4)** 349–354 doi: 10.3103/S1067821213040159
- [22] Gavrilin A et al 2016 *MATEC Web of Conf* **79** 01078 doi: 10.1051/mateconf/20167901078
- [23] Yan X et al Leahy R 1992 *Phys Med Biol* **37(3)** 493–506
- [24] Shishlov A V et al 2000 *Physics of Plasmas* **7(4)** 1252–1262 doi: 10.1063/1.873936